STRUCTURAL BIOLOGY COMMUNICATIONS

ISSN 2053-230X

Ibuprofen: a weak inhibitor of carbonic anhydrase II

Jacob Combs, Jacob Andring and Robert McKenna*

Department of Biochemistry and Molecular Biology, College of Medicine, University of Florida, Gainesville, FL 32610, USA. *Correspondence e-mail: rmckenna@ufl.edu

Received 5 August 2022
Accepted 5 October 2022

Edited by N. Sträter, University of Leipzig, Germany

Keywords: carbonic anhydrases; carboxylic acid-based inhibitors; ibuprofen; X-ray crystallography; kinetics.

PDB reference: carbonic anhydrase II in complex with ibuprofen, 8dj9

Supporting information: this article has supporting information at journals.iucr.org/f

Carbonic anhydrases (CAs) are drug targets for a variety of diseases. While many clinically relevant CA inhibitors are sulfonamide-based, novel CA inhibitors are being developed that incorporate alternative zinc-binding groups, such as carboxylic acid moieties, to develop CA isoform-specific inhibitors. Here, the X-ray crystal structure of human CA II (hCA II) in complex with the carboxylic acid ibuprofen [2-(4-isobutylphenyl)propanoic acid, a common over-the-counter nonsteroidal anti-inflammatory drug] is reported to 1.54 Å resolution. The binding of ibuprofen is overlaid with the structures of other carboxylic acids in complex with hCA II to compare their inhibition mechanisms by direct or indirect (via a water) binding to the active-site zinc. Additionally, enzyme-inhibition assays using ibuprofen, nicotinic acid and ferulic acid were performed with hCA II to determine their IC_{50} values and were compared with those of other carboxylic acid binders. This study discusses the potential development of CA inhibitors utilizing the carboxylic acid moiety.

1. Introduction

Carbonic anhydrases (CAs) are a family of metalloenzymes that catalyze the reversible conversion of carbon dioxide (CO_2) and water to bicarbonate (HCO_3^-) and a proton via a coordinated metal ion (Steiner *et al.*, 1975). Within this family of metalloenzymes, the α-class zinc-containing human CAs are the most widely studied and understood, and include human carbonic anhydrase II (hCA II), which is widespread in many tissue types and is especially prominent in erythrocytes (Frost & McKenna, 2013). The CA mechanism of catalysis occurs in two distinct steps: hydration/dehydration of CO_2 (1) via the zinc-bound solvent (ZBS) and recycling of the ZBS from water to hydroxide (2) via the proton-shuttling residue His64 at the rim of the active site (Fisher *et al.*, 2010):

$$CO_2 + EZnOH^- \longleftrightarrow EZnHCO_3^- \longleftrightarrow EZnH_2O + HCO_3^-, \quad (1)$$

$$EZnH_2O + B \longleftrightarrow EZnOH^- + BH^+. \quad (2)$$

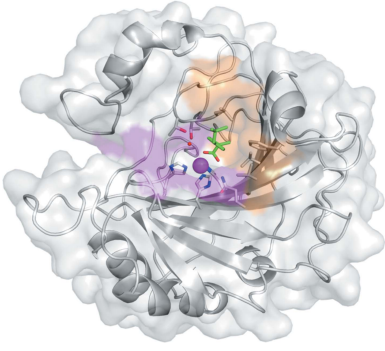

Many of the human CA isoforms have been shown to be therapeutic targets in diseases such as glaucoma, edema and altitude sickness, and are also being developed for the treatment of certain cancers (Combs *et al.*, 2020; Maren, 1967; Supuran, 2008; Frost & McKenna, 2013). Hence, a focus of CA research is on the development of CA inhibitors (CAIs), which dates back to the 1930s. Initial studies demonstrated sulfanilamide (*p*-aminobenzenesulfonamide) to be a potent inhibitor of the enzyme, with its mode of inhibition being directly attributed to the sulfonamide moiety (SO_2NH_2; Keilin & Mann, 1940). In further studies, the development of heterocyclic sulfonamide inhibitors with increased potency

resulted in inhibitors with nanomolar binding constants (Miller *et al.*, 1950). The sulfonamide moiety is known to inhibit CAs by directly binding to the active-site zinc, which is coordinated by three histidines (His94, His96 and His119; hCA II numbering) and a ZBS in a tetrahedral geometry, displacing the catalytic ZBS. The sulfonamide-based CAIs are termed classical CA inhibitors as they are the most widely studied pharmacophore in CAIs (Supuran, 2016). However, there has been a change in emphasis in the last few decades to develop CA isoform-specific inhibitors for the clinical treatment of a variety of diseases, including certain cancers (Bonardi *et al.*, 2022; Bozdag *et al.*, 2014; Mboge *et al.*, 2021; Vannozzi *et al.*, 2022). A major hurdle in the development of effective CAIs is the similarity between the human CA isoforms, which leads to off-target binding. Thus, new isoform-specific CAIs that bind differentially depending on the amino acids that line the active sites are currently under development (Bozdag *et al.*, 2022; Lomelino *et al.*, 2016).

As such, alternative zinc-binding moieties other than sulfonamides are being explored to target the CA active site. Some examples include phenols, polyamines, coumarins, sulfocoumarins and carboxylic acids (Lomelino *et al.*, 2016). Interestingly, not all carboxylic acid-based inhibitors show the same binding mode within the CA active site (Figs. 1*a* and 1*d*; Lomelino & McKenna, 2019). The carboxylic acid inhibitors either bind directly (Figs. 1*b* and 1*e*) or indirectly (Figs. 1*c* and 1*f*) to the zinc. In the case of direct binding, an O atom of the carboxylic acid displaces the catalytic ZBS (Langella *et al.*, 2016) and therefore prevents the first step in the enzymatic mechanism (1), nucleophilic attack of the hydroxide on the CO_2 substrate (Figs. 1*b* and 1*e*; Fisher *et al.*, 2010). In the indirect binding mode, in contrast, the carboxylic acid binds to the zinc via a bridging hydrogen bond to the ZBS (Figs. 1*c* and 1*f*; Lomelino & McKenna, 2019). In this mode, it is thought that the second step in the enzymatic mechanism (2) is blocked, with the inhibitor stabilizing the ZBS, which blocks access to the zinc within the active site.

Ibuprofen, nicotinic acid and ferulic acid are all medically administered enzyme inhibitors that contain a carboxylic acid moiety. Ibuprofen has analgesic, antipyretic and anti-inflammatory properties, which is why it is typically utilized by patients with inflammation and arthritis (Dornan & Reynolds, 1974). Nicotinic acid is typically used to treat dyslipidemia states by increasing the concentration of plasma HDL cholesterol (Bodor & Offermanns, 2008). Ferulic acid has been linked to a wide variety of functions such as anticancer, antimicrobial, antidiabetic, antioxidant and anti-inflammatory properties (Zduńska *et al.*, 2018). Ferulic acid has also been linked to wound healing and enhanced angiogenesis, and is used in cosmetics, food and pharmaceutical applications (Zduńska *et al.*, 2018).

This paper presents the structure of hCA II in complex with the carboxylic acid-based inhibitor ibuprofen determined by X-ray crystallography. In addition, inhibition studies of hCA II with ibuprofen as well as with the carboxylic acid-based compounds nicotinic acid and ferulic acid were performed.

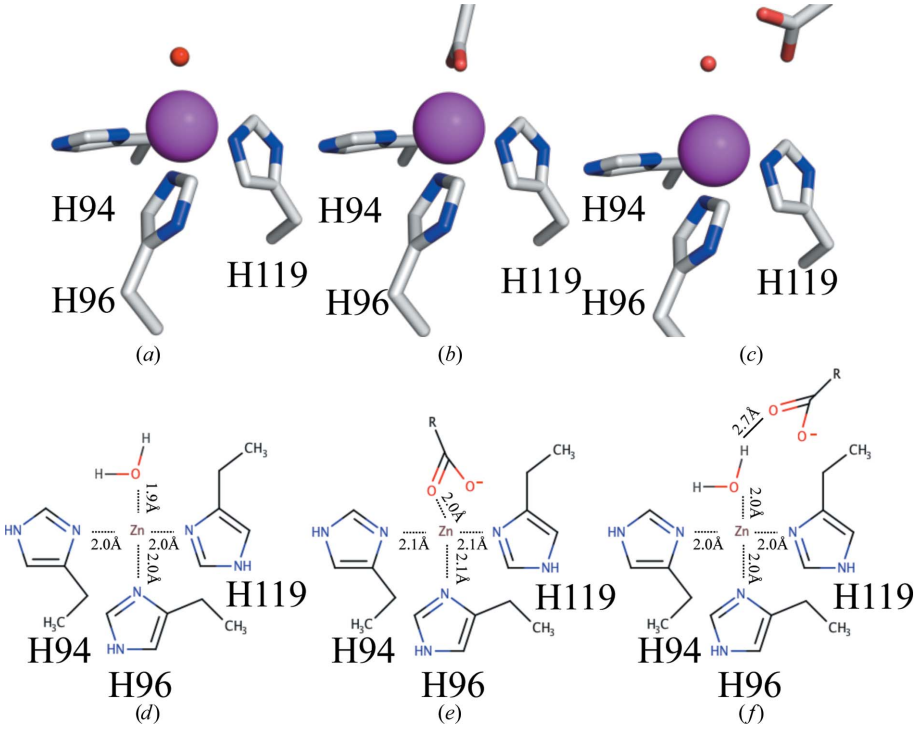

Figure 1
Carboxylic acid inhibitor-binding modes of CA. (*a*), (*b*), (*c*) Observed crystallographic data from PDB entries 3ks3, 8dj9 and 5eh8, respectively; (*d*), (*e*), (*f*) schematic models. (*a*, *d*) hCA II active site with ZBS, (*b*, *e*) direct inhibition in which the carboxylic acid displaces the ZBS and (*c*, *f*) indirect inhibition with the carboxylic acid hydrogen-bonded to the ZBS. (*a*), (*b*), (*c*) Zinc is depicted as a magenta sphere, water as a red sphere, the O atoms of the carboxylic acid moiety of the inhibitor are in red and the active-site histidine residues are labeled. (*d*), (*e*), (*f*) Zinc direct metal coordination is depicted as dashed lines, with hydrogen bonds as solid lines; the respective distances are labeled.

Based on these structural and activity observations, combined with other literature reports, the implications of the direct and indirect binding modes between carboxylic acid-based inhibitors and hCA II are discussed.

2. Materials and methods

2.1. Macromolecule production

The enzyme hCA II was expressed in *Escherichia coli* BL21 pLysS (DE3) cells from New England Biolabs and was purified as described previously (Pinard *et al.*, 2013; Tanhauser *et al.*, 1992). The cells were grown in LB medium (Fisher) and protein expression was induced using 1 m*M* isopropyl β-D-1-thiogalactopyranoside (Fisher) and 1 m*M* zinc sulfate (Fisher) for 3 h (Fisher *et al.*, 2009). The cell pellets were lysed with a microfluidizer (Microfluidics LM10) after harvesting via centrifugation (Beckman J-10). The protein was loaded onto a *p*-aminomethylbenzenesulfonamide–agarose (Sigma) column and hCA II was eluted with 0.4 *M* sodium azide (Fisher). hCA II was buffer-exchanged into 50 m*M* Tris pH 8.0 (Fisher) and concentrated to 10 mg ml^{-1}. The protein purity was checked with by SDS–PAGE (Fisher).

2.2. Crystallization

The crystallization conditions for hCA II were set up as described previously (Lomelino & McKenna, 2019). In brief, a 1:1 ratio of protein (10 mg ml^{-1}) and precipitant solution (1.6 *M* sodium citrate, 50 m*M* Tris pH 7.8) in a drop of 5 µl in volume was suspended over 500 µl precipitant solution (Fisher) by the hanging-drop vapor-diffusion method using a 24-well VDXm Plate with sealant (Hampton Research). The plate was incubated at room temperature and crystal growth was noted within a week. The hCA II crystals were soaked with 1 µl 100 m*M* ibuprofen (Sigma; a final concentration of 17 m*M*) for 1 h prior to crystal mounting. A 20% glycerol (Fisher) precipitant solution was used as a cryoprotectant to transfer the hCA II crystals before flash-cooling in liquid nitrogen.

2.3. Data collection and processing

X-ray crystallographic diffraction data were collected on the BL9-2 beamline at Stanford Synchrotron Radiation Lightsource (SSRL) using a PILATUS 6M detector. An exposure time of 0.5 s, an oscillation angle of 1° and a crystal-to-detector distance of 270 mm were used to collect a 180-image data set. *XDS* was used to index and integrate the diffraction data (Kabsch, 2010) and *AIMLESS* from the *CCP*4 program package was used to reduce and scale the data in space group $P2_1$ (Evans & Murshudov, 2013; Winn *et al.*, 2011). Molecular replacement was performed using the wild-type hCA II structure with PDB code 3ks3 as a search model to determine the initial phases (Avvaru *et al.*, 2010). The interactive graphical software *Coot* (Emsley *et al.*, 2010) was used to modify the model and inspect the electron-density maps, while *Phenix* (Leibschner *et al.*, 2019) was used to refine the model and generate restraint files for ibuprofen. Interactions were determined via *LigPlot* (Laskowski & Swindells, 2011) and figures were generated in *PyMOL* (version 0.9.4; Schrödinger).

Table 1
X-ray crystallographic data-collection and refinement statistics for the hCA II–ibuprofen complex (PDB entry 8dj9).

Values in parentheses are for the highest resolution shell.

Resolution range (Å)	35.0–1.54 (1.60–1.54)
Space group	$P12_11$
a, b, c (Å)	42.7, 41.7, 72.3
α, β, γ (°)	90, 104.2, 90
Total reflections	119485 (8472)
Unique reflections	35621 (3017)
Multiplicity	3.4 (2.8)
Completeness (%)	96.8 (83.0)
Mean $I/\sigma(I)$	18.6 (2.3)
R_{merge}†	0.25 (0.44)
R_{meas}‡	0.30 (0.54)
$R_{p.i.m.}$§	0.16 (0.31)
Reflections used in refinement	35605 (3017)
Reflections used for R_{free}	1779 (144)
R_{work}¶	0.14 (0.18)
R_{free}††	0.17 (0.23)
No. of non-H atoms	
Total	2491
hCA II	2120
Ibuprofen	76
Solvent	327
No. of protein residues	258
R.m.s.d.s	
Bond lengths (Å)	0.01
Angles (°)	1.14
Ramachandran statistics	
Favored (%)	96.5
Allowed (%)	3.5
Outliers (%)	0.0
Average B factors (Å^2)	
Overall	16.9
hCA II	14.9
Ibuprofen	26.8
Solvent	28.7

† $R_{merge} = \sum_{hkl}\sum_i |I_i(hkl) - \langle I(hkl)\rangle| / \sum_{hkl}\sum_i I_i(hkl)$. ‡ $R_{meas} = \sum_{hkl}\{N(hkl)/[N(hkl)-1]\}^{1/2}\sum_i |I_i(hkl) - \langle I(hkl)\rangle| / \sum_{hkl}\sum_i I_i(hkl)$. § $R_{p.i.m.} = \sum_{hkl}\{1/[N(hkl)-1]\}^{1/2}\sum_i |I_i(hkl) - \langle I(hkl)\rangle| / \sum_{hkl}\sum_i I_i(hkl)$. ¶ $R_{work} = \sum_{hkl}\big||F_{obs}| - |F_{calc}|\big| / \sum_{hkl}|F_{obs}|$. †† $R_{free} = \sum_{hkl}\big||F_{obs}| - |F_{calc}|\big| / \sum_{hkl}|F_{obs}|$ (using data omitted from refinement (5%).

2.4. Kinetics

A colorimetric substrate, 4-nitrophenyl acetate (pNPA), was used to perform esterase assays that measured the inhibition constants of ibuprofen, nicotinic acid (Acros Organics) and ferulic acid (Sigma) in the presence of hCA II. An ester bond within pNPA (Sigma) is cleaved by hCA II, forming 4-nitrophenol that absorbs strongly at 348 nm. This allows the reaction to be monitored spectroscopically (Tashian *et al.*, 1964). Inhibition experiments varied the concentrations of ibuprofen, nicotinic acid and ferulic acid between 2 and 50 m*M*. These inhibitors were incubated with 50 µl 0.1 mg ml^{-1} hCA II at room temperature for 30 min. 200 µl of 3 m*M* pNPA in 3% acetone (Sigma) was added to the sample and immediately scanned in a Synergy HTX BioTek plate reader at 348 nm absorbance for 10 min. Acetazolamide (Sigma) was used as a positive control for inhibition. The data

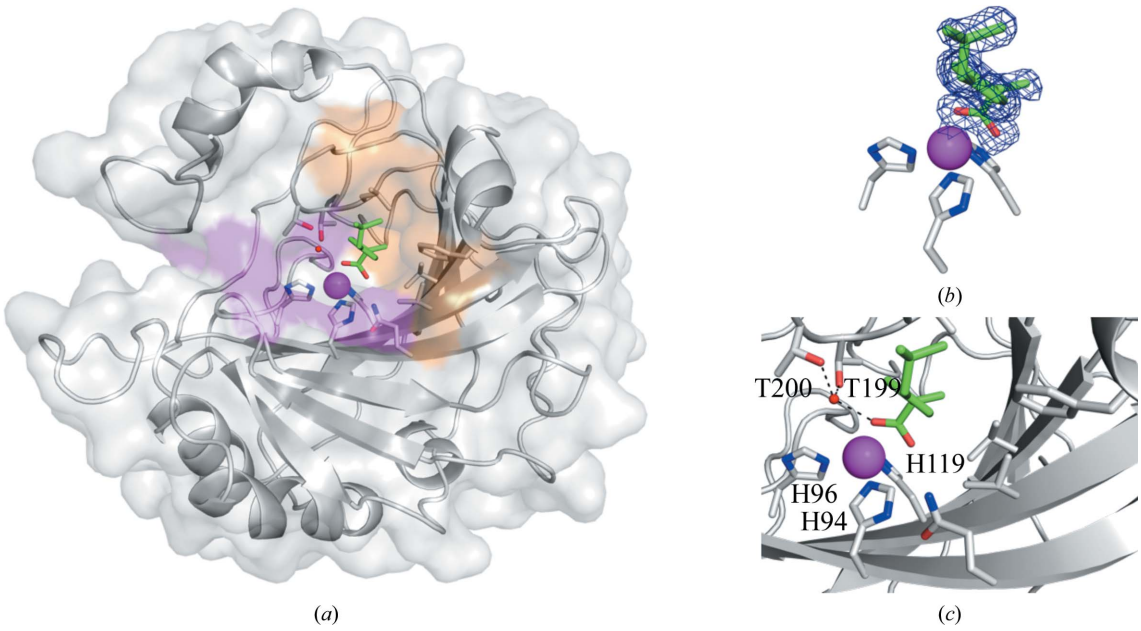

Figure 2
Structure of hCA II in complex with ibuprofen. (*a*) Surface view of the complex, with the hydrophobic face of the hCA II active site in orange, the hydrophilic face in purple and ibuprofen in green. (*b*) Close-up of the ibuprofen binding site with a $2F_o - F_c$ electron-density mesh (blue, contoured at 1.0σ). (*c*) Interactions of ibuprofen with relevant hCA II residues as labeled. Hydrogen bonds are shown as dashed lines, waters as red spheres, zinc ions as magenta spheres and bound ibuprofen as green sticks.

were analyzed using *Prism* (version 9.2.0; GraphPad). A line of best fit was fitted to the data.

3. Results

3.1. X-ray crystallography

The crystal structure of hCA II in complex with ibuprofen was determined to a resolution of 1.54 Å and deposited in the PDB as entry 8dj9 (Table 1, Fig. 2). While ibuprofen exists as two isomers (*R* and *S*), only the *S* isomer binds to hCA II. This is important as this is the pharmacologically active isomer (Geisslinger *et al.*, 1989).

For the inhibition of hCA II by ibuprofen, the carboxylic acid directly binds to the zinc and displaces the ZBS (Fig. 2*b*). This binding mode is similar to that in previously described direct complexes of carboxylic acid-based inhibitors with hCA II (Boone *et al.*, 2014). The ibuprofen binds between the hydrophobic and hydrophilic sides of the active site. The hydrophilic residues Thr199 and Thr200 form hydrogen bonds to a water within the active site that also forms a hydrogen bond to the carboxylic acid of ibuprofen (Fig. 2*c*). The hydrophobic residues Val121, Phe131, Val143, Leu198 and Trp209 and the hydrophilic residue Gln92 all make significant intermolecular interactions with the ring and tail portion of ibuprofen (Fig. 2*c*). Hence, ibuprofen predominately interacts within the hydrophobic pocket of hCA II, with an occluded interface binding surface area of 240 Å^2 (Table 2).

3.2. Inhibition

In addition to the interconversion of CO_2 and HCO_3^-, hCA II also has an esterase activity that can be used as a CA functional assay (Tashian *et al.*, 1964). A colorimetric probe such as 4-nitrophenyl acetate (pNPA) is used as a substrate to monitor the reaction when the enzyme cleaves the ester bond to form 4-nitrophenyl, which is spectroscopically absorbent at 348 nm (Bua *et al.*, 2020; Uda *et al.*, 2015). This assay was used to measure the catalytic rate of the enzyme in the presence of ibuprofen, nicotinic acid and ferulic acid. The three inhibitors were initially tested at concentrations of 50, 30, 20, 10, 5 and 2 m*M*. Additional experiments were performed between concentrations of 2 and 20 m*M* to obtain further data points near the 50% inhibition concentration. The data were plotted

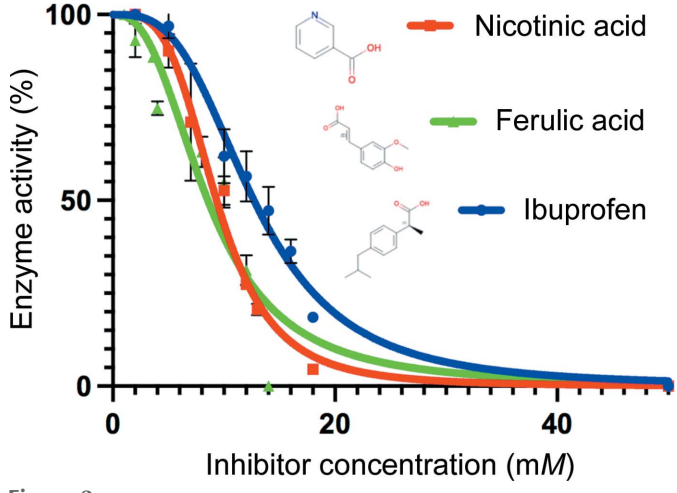

Figure 3
Inhibition of hCA II with ibuprofen (blue circles), nicotinic acid (red squares) and ferulic acid (green triangles). Each compound concentration was run in triplicate; error bars indicate standard deviations. Where error bars are not present the standard deviation is too small for the software to depict. The chemical structures of each compound are shown in the inset.

Table 2
Carboxylic acid structures in complex with hCA II in the PDB.

Compound	Binding mode	Inhibition (K_i, K_d or IC_{50})	PDB code	Interface area (Å^2)	Zinc to carboxylate (Å)	Zinc to H_2O (Å)	H_2O to carboxylate (Å)	Reference
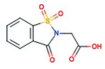	Direct (class II)	K_i = 80 µ*M*	5clu	216	2.0	N/A	N/A	Langella *et al.* (2016)
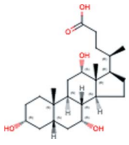	Direct (class I)	IC_{50} = 0.2 m*M*	4n16	322	2.1	N/A	N/A	Boone *et al.* (2014)
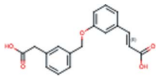	Direct (class I)	K_d = 0.8 m*M*	5ehv	263	2.0	N/A	N/A	Woods *et al.* (2016)
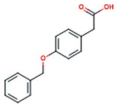	Direct (class II)	K_d = 1.1 m*M*	5flq	256	1.9	N/A	N/A	Woods *et al.* (2016)
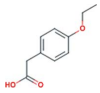	Direct (class I)	K_d = 5.2 m*M*	5fnj	227	2.0	N/A	N/A	Woods *et al.* (2016)
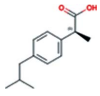	Direct (class II)	IC_{50} = 13 m*M*	8dj9	239	2.0	N/A	N/A	This work
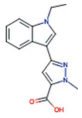	Indirect	K_i = 0.8 µ*M*	6b4d	263	3.7	2.0	2.7	Cadoni *et al.* (2017)
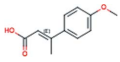	Indirect	K_d = 0.8 m*M*	5eh8	222	3.7	2.0	2.7	Woods *et al.* (2016)
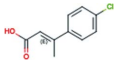	Indirect	K_d = 0.9 m*M*	5fls	206	3.7	2.0	2.7	Woods *et al.* (2016)
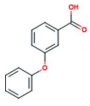	Indirect	K_d = 1.3 m*M*	5flt	234	3.6	2.0	2.6	Woods *et al.* (2016)
	Indirect	IC_{50} = 3 m*M*	4e3f	187	4.2	2.1	2.6	Martin & Cohen (2012)
	Indirect	IC_{50} = 5 m*M*	4e3d	182	3.7	2.0	2.6	Martin *et al.* (2012)
	Indirect	IC_{50} = 6.6 m*M*	6ux1	177	3.7	2.1	2.5	Andring *et al.* (2020)
	Indirect	IC_{50} = 8 m*M*	4e3g	175	3.6	2.2	3.0	Martin & Cohen (2012)
	Indirect	IC_{50} = 9 m*M*	4e4a	183	3.6	2.1	2.7	Martin & Cohen (2012)
	Indirect	IC_{50} = 10 m*M*	6mbv	164	3.6	2.1	2.6	Lomelino & McKenna (2019)
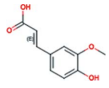	Indirect	IC_{50} = 10 m*M*	6mby	229	3.6	2.1	2.5	Lomelino & McKenna (2019)

to a nonlinear regression using *Prism* to determine IC_{50} values (Fig. 3). The average standard deviations at each concentration for ibuprofen, nicotinic acid and ferulic acid are 3.5, 3.4 and 2.8% of the enzyme activity, respectively. The calculated IC_{50} values of ibuprofen, nicotinic acid and ferulic acid are 12.8 ± 1.1, 9.6 ± 1.0 and 10.6 ± 1.0 m*M*, respectively, with a 95% confidence interval. The lines of best fit for all three inhibitors have an R^2 value above 0.94.

4. Discussion

In this study, the structure of hCA II in complex with ibuprofen has been determined to 1.54 Å resolution using X-ray crystallography (Fig. 2). Esterase inhibition activity studies were used to obtain the IC_{50} values for ibuprofen, nicotinic acid and ferulic acid, which were determined to be 15.3, 10.4 and 8.6 m*M*, respectively (Fig. 3). Unlike nicotinic acid and ferulic acid, ibuprofen has a chiral branch between the carboxylic acid and benzene ring moieties which creates some slight steric binding issues within the active site of hCA II. Additionally, ibuprofen binds directly to the zinc, displacing the ZBS. On the other hand, both nicotinic acid and ferulic acid do not have a chiral branch linker and bind through a hydrogen bond to the ZBS, rather than directly to the zinc (Lomelino & McKenna, 2019). These differences in both the conformational nature and the binding mode contribute to the weaker binding of ibuprofen. These observations lead to the hypothesis that one or either of these features may account for the differences in CA inhibition between the three carboxylic acid-based compounds studied here and previously.

While hCA II is not the target of ibuprofen in a treatment regimen, it does bind at concentrations that are physiologically relevant. With a standard dose of 200 mg and with the average human having 5 l of blood (Cooper *et al.*, 1977; Dean, 2005), the effective physiological concentration of ibuprofen in the blood would be ~0.2 m*M*. Considering the calculated IC_{50} of 13 m*M*, it is unlikely that much ibuprofen would bind to hCA II *in vivo*. As such, no side effects would be expected due to interactions with hCA II.

To further investigate the carboxylic acid binding modes, the structures of an additional 15 carboxylic acid moiety-based hCA II inhibitors were examined. Analysis of the PDB (Berman *et al.*, 2003) revealed that the carboxylic acid

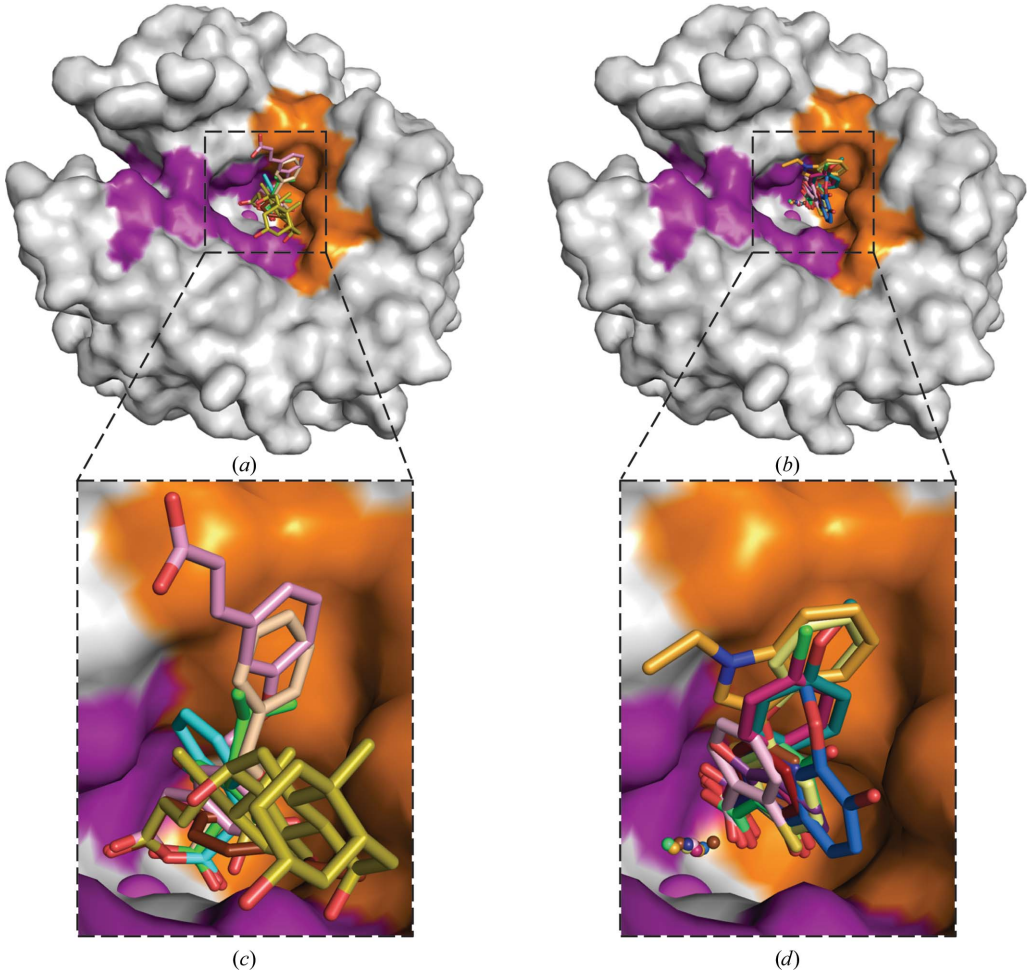

Figure 4
Carboxylic acid inhibitor–hCA II complex structures. (*a*) Superposition of direct binding to the zinc: ibuprofen (green; PDB entry 8dj9), saccharin derivative (teal; PDB entry 5clu), an ethanoic acid derivative (chocolate; PDB entry 5fnj), another ethanoic acid derivative (wheat; PDB entry 5flq), propenoic acid (pink; PDB entry 5ehv) and cholate (olive; PDB entry 4n16). (*b*) Superposition of indirect binding via the ZBS: heteroaryl-pyrazole carboxylic acid derivative (orange; PDB entry 6b4d), an enoic acid derivative (deep teal; PDB entry 5eh8), another enoic acid derivative (warm pink; PDB entry 5fls), 3-phenoxybenzoic acid (pale yellow; PDB entry 5flt), 2,6-dihydroxybenzoic acid (violet purple; PDB entry 4e3f), 2,5-dihydroxybenzoic acid (lemon; PDB entry 4e3d), *p*-hydroxybenzoic acid (lime green; PDB entry 4e3g), 2-sulfanylbenzoic acid (light pink; PDB entry 4e4a), ferulic acid (marine; PDB entry 6mby), nicotinic acid (deep blue; PDB entry 6mbv), salicylic acid (dark red; PDB entry 6ux1) and 2-hydroxybenzoic acid (brown; PDB entry 5m78). (*c*) and (*d*) are active-site close-up views of (*a*) and (*b*), respectively. Zinc is shown as a magenta sphere, the hydrophobic pocket is in orange and the hydrophilic pocket is in purple with PDB codes included for reference.

compounds followed the direct and indirect binding modes described here. Ibuprofen (this study; green; PDB entry 8dj9), a saccharin derivative (teal; PDB entry 5clu), an ethanoic acid derivative (chocolate; PDB entry 5fnj), another ethanoic acid derivative (wheat; PDB entry 5flq), propenoic acid (pink; PDB entry 5ehv) and cholate (olive; PDB entry 4n16) bound via direct binding to the zinc (Boone *et al.*, 2014; Langella *et al.*, 2016; Woods *et al.*, 2016; Fig. 4*a*). In contrast, a heteroaryl-pyrazole carboxylic acid derivative (orange; PDB entry 6b4d), an enoic acid derivative (deep teal; PDB entry 5eh8), another enoic acid derivative (warm pink; PDB entry 5fls), 3-phenoxybenzoic acid (pale yellow; PDB entry 5flt), 2,6-dihydroxybenzoic acid (violet purple; PDB entry 4e3f), 2,5-dihydroxybenzoic acid (lemon; PDB entry 4e3d), *p*-hydroxybenzoic acid (lime green; PDB entry 4e3g), 2-sulfanylbenzoic acid (light pink; PDB entry 4e4a), ferulic acid (marine; PDB entry 6mby), nicotinic acid (deep blue; PDB entry 6mbv), salicylic acid (dark red; PDB entry 6ux1) and 2-hydroxybenzoic acid (brown; PDB entry 5m78) were observed to bind indirectly to the ZBS (Andring *et al.*, 2020; Cadoni *et al.*, 2017; Lomelino & McKenna, 2019; Martin & Cohen, 2012; Woods *et al.*, 2016; Fig. 4*b*). Ibuprofen (this study; green) almost superimposed onto the previously determined structure of cholic acid (olive) bound to hCA II (Boone *et al.*, 2014; Fig. 4*a*).

Upon closer inspection, the hCA II direct zinc binders revealed two subgroups with distinctive orientations, with propenoic acid (pink), one ethanoic acid derivative (chocolate) and cholate (olive) binding in one orientation (class I), while ibuprofen (green), the other ethanoic acid derivative (wheat) and the saccharin derivative (teal) bind in a second orientation (class II) in the active site (Fig. 4*c*). In contrast, the indirect binders vary in location and orientation depending on their tail group; the carboxylic acid moieties all bind in the same orientation, with a movement of up to 1.7 Å between the ZBS of different indirect binders (Fig. 4*d*). Overall, the carboxylic acid-based compounds tend to bind predominately

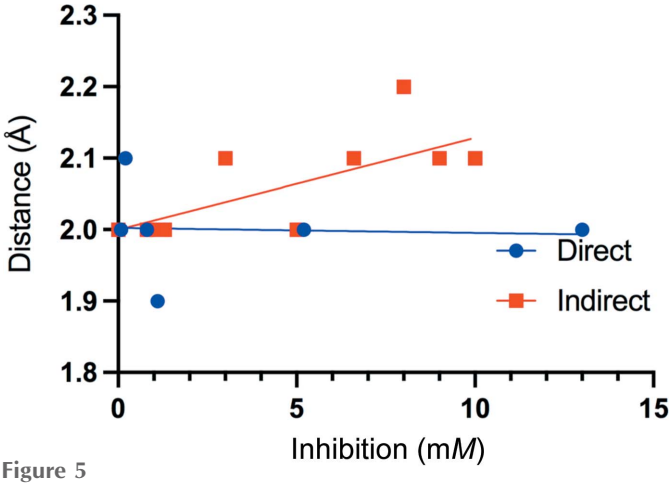

Figure 5
Inhibition of hCA II by carboxylic acid compounds. Inhibition constants previously reported as IC_{50}, K_i or K_d versus active-site distance. Direct binders are shown as blue circles and indirect binders as red squares. For direct binders the distance from the zinc to the closest O atom in the carboxyl group is measured, while for indirect binders the distance from the ZBS to the zinc is measured.

on the hydrophobic side as opposed to the hydrophilic side of the active-site cavity (Figs. 4*b* and 4*d*).

When studying enzyme inhibition, the technique and the reported kinetic value can differ depending on the equipment and the assay used by the researchers. There are a variety of reportable constants related to inhibitor binding such as K_i (the inhibition constant), IC_{50} (the half-maximal inhibitory concentration) and K_d (the dissociation constant) (Table 2). These values can be compared using the equation $K_i = IC_{50}/\{1 + ([C]/K_d)\}$. Taking the inhibition data for carboxylic acid hCA II binders from the literature, the direct binders have an average kinetic inhibition (K_i) of 3.4 ± 5.1 m*M*, while the indirect binders have an average kinetic inhibition value of 5.5 ± 3.8 m*M* (excluding the lowest value of 0.8 μ*M*, which is 1000-fold lower than the second lowest kinetic value and is associated with a heteroaryl-pyrazole carboxylic acid derivative; PDB entry 6b4d). Therefore, on average the direct binders have a slightly higher affinity for CA compared with the indirect binders, although this difference is not statistically significant. This difference might be due to the carboxylic acid having a higher affinity for zinc than for the ZBS. Furthermore, the carboxylic acid inhibitors are identifed as weak binders; the commonly used sulfonamide hCA II inhibitor acetazolamide has a K_i value of 10 n*M* (Supuran *et al.*, 2003).

In broad terms, the higher the indirect carboxylic acid affinity, the larger the covered interface area between the compound and the active-site residues (Table 2). However, no trend is observed for the direct binders, which might be because of the smaller sample size of the structures. The average interface between hCA II and direct and indirect binders is 260 ± 40 and 200 ± 30 $Å^2$, respectively. This demonstrates that the direct binders interact more strongly with residues within the active site than indirect binders. This is attributed to the direct binders being buried further within the active-site pocket compared with the indirect binders.

For the indirect carboxylic acid binders, the distance between the zinc and ZBS is shorter for the tighter binders and larger for the weaker binders (Fig. 5, Table 2). However, this trend is less convincing for the direct binders. For the indirect binders the K_i for hCA II increases as the compounds move slightly farther away from the zinc.

The average distance between the O atom of the carboxylic acid group of indirect binders and the ZBS is 2.7 Å, while the distance between the zinc and the O atom of the carboxylic acid group of indirect binders is 3.7 Å. In contrast, the average distance between the O atom of the carboxylic acid group of direct binders and the zinc is 2.0 Å. The distance between the ZBS and the zinc for indirect binders is slightly greater at 2.06 Å (Table 2). This small increase in distance between ZBS and zinc seen in indirect binders could be the rationale for their weaker affinities compared with direct binders.

These data provide information for the design of alternative zinc-binding groups: carboxylic acid moieties for CA inhibitors rather than the classical sulfonamide drugs currently in clinical use. While the sulfonamide-based compounds are several logs better at inhibiting than carboxylic acids, the carboxylic acid-based inhibitors rely less on their affinity to

bind zinc and more on their interactions with the amino acids that line the active site, giving them greater design potential to better target selection between the different CA isoforms.

Acknowledgements

Experiments were performed at SSRL and the authors would like to acknowledge the guidance and expertise of the SSRL staff.

References

Andring, J., Combs, J. & McKenna, R. (2020). *Biomolecules*, **10**, 527.
Avvaru, B. S., Kim, C. U., Sippel, K. H., Gruner, S. M., Agbandje-McKenna, M., Silverman, D. N. & McKenna, R. (2010). *Biochemistry*, **49**, 249–251.
Berman, H. M., Henrick, K. & Nakamura, H. (2003). *Nat. Struct. Mol. Biol.* **10**, 980.
Bodor, E. T. & Offermanns, S. (2008). *Br. J. Pharmacol.* **153**, S68–S75.
Bonardi, A., Bua, S., Combs, J., Lomelino, C., Andring, J., Osman, S. M., Toti, A., Di Cesare Mannelli, L., Gratteri, P., Ghelardini, C., McKenna, R., Nocentini, A. & Supuran, C. T. (2022). *J. Enzyme Inhib. Med. Chem.* **37**, 930–939.
Boone, C. D., Tu, C. & McKenna, R. (2014). *Acta Cryst.* D**70**, 1758–1763.
Bozdag, M., Cravey, L., Combs, J., Kota, A., McKenna, R., Angeli, A., Selleri, S., Carta, F. & Supuran, C. T. (2022). *ChemMedChem*, **17**, e202200148.
Bozdag, M., Ferraroni, M., Nuti, E., Vullo, D., Rossello, A., Carta, F., Scozzafava, A. & Supuran, C. T. (2014). *Bioorg. Med. Chem.* **22**, 334–340.
Bua, S., Lomelino, C., Murray, A. B., Osman, S. M., ALOthman, Z. A., Bozdag, M., Abdel-Aziz, H. A., Eldehna, W. M., McKenna, R., Nocentini, A. & Supuran, C. T. (2020). *J. Med. Chem.* **63**, 321–333.
Cadoni, R., Pala, N., Lomelino, C., Mahon, B. P., McKenna, R., Dallocchio, R., Dessì, A., Carcelli, M., Rogolino, D., Sanna, V., Rassu, M., Iaccarino, C., Vullo, D., Supuran, C. T. & Sechi, M. (2017). *ACS Med. Chem. Lett.* **8**, 941–946.
Combs, J. E., Andring, J. T. & McKenna, R. (2020). *Methods Enzymol.* **634**, 281–309.
Cooper, S. A., Needle, S. E. & Kruger, G. O. (1977). *J. Oral Surg.* **35**, 898–903.
Dean, L. (2005). *Blood Groups and Red Cell Antigens*, ch. 1. Bethesda: National Center for Biotechnology Information.
Dornan, J. & Reynolds, W. J. (1974). *Can. Med. Assoc. J.* **110**, 1370–1372.
Emsley, P., Lohkamp, B., Scott, W. G. & Cowtan, K. (2010). *Acta Cryst.* D**66**, 486–501.
Evans, P. R. & Murshudov, G. N. (2013). *Acta Cryst.* D**69**, 1204–1214.
Fisher, S. Z., Kovalevsky, A. Y., Domsic, J. F., Mustyakimov, M., McKenna, R., Silverman, D. N. & Langan, P. A. (2010). *Biochemistry*, **49**, 415–421.
Fisher, S. Z., Kovalevsky, A. Y., Domsic, J. F., Mustyakimov, M., Silverman, D. N., McKenna, R. & Langan, P. (2009). *Acta Cryst.* F**65**, 495–498.
Frost, S. C. & McKenna, R. (2013). *Carbonic Anhydrase: Mechanism, Regulation, Links to Disease, and Industrial Applications*. Dordrecht: Springer.
Geisslinger, G., Stock, K. P., Bach, G. L., Loew, D. & Brune, K. (1989). *Agents Actions*, **27**, 455–457.
Kabsch, W. (2010). *Acta Cryst.* D**66**, 125–132.
Keilin, D. & Mann, T. (1940). *Biochem. J.* **34**, 1163–1176.
Langella, E., D'Ambrosio, K., D'Ascenzio, M., Carradori, S., Monti, S. M., Supuran, C. T. & De Simone, G. (2016). *Chem. Eur. J.* **22**, 97–100.
Laskowski, R. A. & Swindells, M. B. (2011). *J. Chem. Inf. Model.* **51**, 2778–2786.
Liebschner, D., Afonine, P. V., Baker, M. L., Bunkóczi, G., Chen, V. B., Croll, T. I., Hintze, B., Hung, L.-W., Jain, S., McCoy, A. J., Moriarty, N. W., Oeffner, R. D., Poon, B. K., Prisant, M. G., Read, R. J., Richardson, J. S., Richardson, D. C., Sammito, M. D., Sobolev, O. V., Stockwell, D. H., Terwilliger, T. C., Urzhumtsev, A. G., Videau, L. L., Williams, C. J. & Adams, P. D. (2019). *Acta Cryst.* D**75**, 861–877.
Lomelino, C. L. & McKenna, R. (2019). *Acta Cryst.* F**75**, 166–170.
Lomelino, C., Supuran, C. & McKenna, R. (2016). *Int. J. Mol. Sci.* **17**, 1150.
Maren, T. H. (1967). *Physiol. Rev.* **47**, 595–781.
Martin, D. P. & Cohen, S. M. (2012). *Chem. Commun.* **48**, 5259–5261.
Mboge, M. Y., Combs, J., Singh, S., Andring, J., Wolff, A., Tu, C., Zhang, Z., McKenna, R. & Frost, S. C. (2021). *J. Med. Chem.* **64**, 1713–1724.
Miller, W. H., Dessert, A. M. & Roblin, R. O. (1950). *J. Am. Chem. Soc.* **72**, 4893–4896.
Pinard, M. A., Boone, C. D., Rife, B. D., Supuran, C. T. & McKenna, R. (2013). *Bioorg. Med. Chem.* **21**, 7210–7215.
Steiner, H., Jonsson, B.-H. & Lindskog, S. (1975). *Eur. J. Biochem.* **59**, 253–259.
Supuran, C. T. (2008). *Nat. Rev. Drug Discov.* **7**, 168–181.
Supuran, C. T. (2016). *J. Enzyme Inhib. Med. Chem.* **31**, 345–360.
Supuran, C. T., Scozzafava, A. & Casini, A. (2003). *Med. Res. Rev.* **23**, 146–189.
Tanhauser, S. M., Jewell, D. A., Tu, C. K., Silverman, D. N. & Laipis, P. J. (1992). *Gene*, **117**, 113–117.
Tashian, R. E., Douglas, D. P. & Yu, Y. L. (1964). *Biochem. Biophys. Res. Commun.* **14**, 256–261.
Uda, N. R., Seibert, V., Stenner-Liewen, F., Müller, P., Herzig, P., Gondi, G., Zeidler, R., van Dijk, M., Zippelius, A. & Renner, C. (2015). *J. Enzyme Inhib. Med. Chem.* **30**, 955–960.
Vannozzi, G., Vullo, D., Angeli, A., Ferraroni, M., Combs, J., Lomelino, C., Andring, J., McKenna, R., Bartolucci, G., Pallecchi, M., Lucarini, L., Sgambellone, S., Masini, E., Carta, F. & Supuran, C. T. (2022). *J. Med. Chem.* **65**, 824–837.
Winn, M. D., Ballard, C. C., Cowtan, K. D., Dodson, E. J., Emsley, P., Evans, P. R., Keegan, R. M., Krissinel, E. B., Leslie, A. G. W., McCoy, A., McNicholas, S. J., Murshudov, G. N., Pannu, N. S., Potterton, E. A., Powell, H. R., Read, R. J., Vagin, A. & Wilson, K. S. (2011). *Acta Cryst.* D**67**, 235–242.
Woods, L. A., Dolezal, O., Ren, B., Ryan, J. H., Peat, T. S. & Poulsen, S.-A. (2016). *J. Med. Chem.* **59**, 2192–2204.
Zduńska, K., Dana, A., Kolodziejczak, A. & Rotsztejn, H. (2018). *Skin Pharmacol. Physiol.* **31**, 332–336.